Microscopic Mechanism of Ultrafast Excited-State Intramolecular Proton Transfer: A 30-fs Study of 2-(2′-Hydroxyphenyl)benzothiazole†

Stefan Lochbrunner, Alexander J. Wurzer, and Eberhard Riedle*

Lehrstuhl für BioMolekulare Optik, Sektion Physik, Ludwig-Maximilians-Universität, Oettingenstrasse 67, D-80538 München, Germany

Received: May 4, 2003; In Final Form: September 24, 2003

A detailed analysis of the excited-state intramolecular proton transfer (ESIPT) of 2-(2′-hydroxyphenyl)-benzothiazole and the associated wave packet motion is presented. It is based on the evolution of the emission spectrum observed by UV−vis pump−probe absorption measurements with a cross correlation of 35 fs. The rise of the emission is delayed by 33 fs and reveals the time the wave packet needs to evolve along the reaction coordinate. Four decisive molecular motions and their role during the process are identified by the frequencies and phases extracted from the oscillatory signal contributions. A novel model is developed that describes the ESIPT as a ballistic wave packet motion consisting of three major components: First, the H-chelate ring contracts by in-plane bending of the whole molecule, resulting in an acceleration along the corresponding normal mode. The time scale of the motion is given by the inertia of the participating atoms. When the ON distance is sufficiently shortened, the electronic configuration changes, new bonds are formed, and a new equilibrium geometry results. The molecule is now displaced with respect to this geometry and begins to oscillate in those modes that have large projections on the displacement. The proton is shifted passively toward the nitrogen by the initial contraction of the ring and stays there because of the electronic configuration change.

I. Introduction

Inter- and intramolecular proton transfer are fundamental reactions in chemistry and biology that have been extensively investigated.[1−4] A broad class of molecules that contain an H-chelate ring exhibit both in the gas phase and in nonpolar solvents fast excited-state intramolecular proton transfer (ESIPT).[5−7]

From the observation of the unusually large Stokes shift in salicylic acid and its methyl ester, Weller concluded for the first time that proton transfer is occurring in the electronically excited state of these compounds.[8] After photoexcitation, the covalent bond between the proton and the oxygen in the chelate ring is reduced to a hydrogen bond, and simultaneously the original hydrogen bond to a nitrogen or oxygen on the opposite side of the ring is strengthened. This reaction is depicted in Figure 1 for 2-(2′-hydroxyphenyl)benzothiazole (HBT), the compound investigated in the present study. The fluorescence spectrum of HBT dissolved in cyclohexane shows the large Stokes shift characteristic for ESIPT whereas the fluorescence spectrum in ethanol is the mirror image of the absorption spectrum. The apparent lack of ESIPT in ethanol is due to intermolecular hydrogen bonds to solvent molecules.[9] From the comparison of the two fluorescence spectra, a red shift of about 7500 cm^{-1} due to the ESIPT can be estimated. The proposed proton-transfer reaction was confirmed by time-resolved IR spectroscopy that showed the disappearance of the OH stretching vibration while the NH and a C═O stretching vibration emerge.[10]

A large number of studies dealt with the dynamics of the ESIPT. For ESIPT systems with an asymmetric potential energy surface (PES), a time scale of 100 fs was found for various molecules,[11−14] and similarly fast times were even determined at cryogenic temperatures.[6] Because of the small proton mass, it was argued that this is still too slow for a motion of the proton along a barrierless PES.[12] However, a thermally activated crossing of a barrier is in contradiction to the observation of ESIPT at cryogenic temperatures. A key question is therefore whether tunneling of the proton through a significant barrier is a central step of the ESIPT. So far, no deuterium effect has been observed in dedicated investigations.[12,14,15]

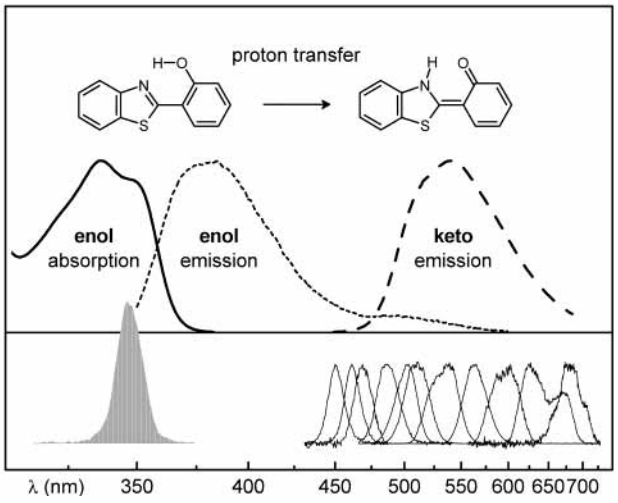

Figure 1. Structure of the enol and keto forms of HBT. Absorption (−) and fluorescence spectrum of HBT in cyclohexane (− − −) and in ethanol (- - -). The lower panel shows the spectrum of the pump pulses (gray fill) and the spectra of the probe pulses for the various center wavelengths used in the time-resolved transmission measurements.

† Part of the special issue "Charles S. Parmenter Festschrift".

* Corresponding author. E-mail: riedle@physik.uni-muenchen.de. Phone: +49-89-2180-9210.

10.1021/jp035203z CCC: $25.00
Published on Web 11/05/2003

The CW absorption and fluorescence spectra consist in general only of broad structures, but some of them show low-frequency progressions at cold temperatures.[13,16] This stimulated the idea of low-frequency vibrations taking part in the ESIPT and determining its time scale.[11−13] A 2D model for the ESIPT of 2-(2′-hydroxyphenyl)benzoxazole (HBO) was developed by Arthen-Engeland et al.[13] and applied to other systems by Douhal et al.[7] The low-frequency vibration is thought to periodically modulate the distance between the proton-donating oxygen and the proton-accepting nitrogen. If the distance is sufficiently shortened, then the barrier for the proton is decreased to a large extent, and a very effective proton-transfer or tunneling process is possible.

For 2-(2′-hydroxy-5′-methylphenyl)benzotriazole (TINUVIN P), Chudoba et al. observed for the first time oscillatory signal contributions associated with the ESIPT.[17] They identified them as coherent vibrational motion in two low-frequency modes at 250 and 470 cm^{-1}, a translational motion of the triazole and the phenyl moieties against each other and a geared in-plane rotation of the two subunits. The modulation of the proton-transfer barrier was attributed to the geared in-plane rotation. Much more pronounced oscillations due to four different modes were presented in a preliminary report of the present work on HBT.[18] Recently, similar low-frequency modes were also detected for 1,8-dihydroxyanthraquinone[19] and 2,5-bis(2'-benzoxazolyl)hydroquinone[20] and even in the time-resolved vibrational spectroscopy of HBT.[21]

The irreversibility and efficiency of the ESIPT are difficult to explain by a model consisting of only one low-frequency mode and one high-frequency proton mode because during every period of the low-frequency vibration the barrier is suppressed and a back transfer of the proton could occur. As discussed below, this inconsistency can be resolved by assuming that a couple of low-frequency modes are directly involved in the ESIPT. In view of the demonstrated importance of low-frequency vibrations, the question arises, which are the relevant vibrational modes, and what is their precise function during the ESIPT?

Theoretical studies of various ESIPT molecules[22−28] are able to reproduce the spectral properties of the compounds. They find that in the excited keto configuration the bond lengths change according to the exchange of single- and double-bond character and the distance between the proton donor and acceptor is slightly reduced in comparison to those of the enol ground state. Electron correlation effects have to be included in the calculations, making them a very challenging task.[27,28] In the accompanying paper, a set of high-level ab initio calculations is presented that for the first time can capture the relevant features of the PES in the transition region for molecules the size of HBT with sufficient accuracy.[29] These and previous results uniformly point to a significant temporary shortening of the donor−acceptor distance when the proton is midway between them.[22−25,30] It was also argued that this shortening is mainly due to a bending mode of the skeleton.[25]

The observation of weak oscillatory signal components in the case of TINUVIN P indicates that the relevant vibrational modes can lead to observable signatures in pump−probe experiments. Our newly developed pump−probe spectrometer[31,32] provides increased temporal resolution and wide tunability of the visible probe pulses. We were therefore able to observe strongly modulated transients for HBT at all emission wavelengths and to attribute them unequivocally to the reactive dynamics in the electronically excited state.[18] Contrary to the case of TINUVIN P where the wave packet motion is masked by the ultrafast electronic decay,[17] our model system HBT has an excited-state lifetime of some 100 ps [33] and is therefore well suited for the observation of vibronic wave packets.

Our goal is to identify the nuclear coordinates taking part in the ESIPT and to clarify their role in the process. From this information, a novel model for the reaction mechanism will arise. Part of the experimental data has already been presented together with a preliminary interpretation.[18] In this paper, we present a detailed analysis of the full data set that reveals the temporal evolution of the ESIPT as well as the vibrational modes that are involved in the process and compose the reaction coordinate. After the description of the experiment in section II, the data and their analysis are presented in section III. In section IV, we discuss the information about the ESIPT that can be deduced from the new experimental data. It is argued that an essentially barrierless PES leads to a ballistic wave packet motion and that the observed oscillatory signal contributions reveal which molecular motions contribute to the reaction coordinate. Direct experimental evidence that the skeletal bending of the molecule induces the transfer is given for the first time. A new multidimensional ESIPT model is presented in section V, which describes the bond change not as tunneling of the proton but as an electronic configuration change that occurs in a transient geometry during an extremely short time interval and leads to the coherent excitation of additional skeletal modes. A short summary of our results is finally given in section VI.

II. Experiment

The ESIPT of HBT was investigated by pump−probe spectroscopy with a time resolution of 30 fs. HBT was excited by pump pulses at 347 nm close to the first maximum of the S_1-S_0 absorption band. The transmission changes induced by the subsequent processes were probed in the wavelength region between 450 and 680 nm covering almost the entire CW fluorescence spectrum. Both the spectrum of the pump pulses and the spectra of the various probe pulses are shown in Figure 1 in comparison to the CW spectra of HBT.

The fully tunable pump−probe spectrometer is based on two NOPAs[31,34] pumped by a home-built Ti:sapphire laser system. The pump pulses were generated by frequency doubling and recompression of the output of one of the NOPAs and had a duration of 25 fs. Their energy was adjusted to about 20 nJ at the sample to excite 2% of the molecules in a focus of 100-μm diameter. The tunable probe pulses stemming from the second NOPA were about 10 times weaker at the sample and had a pulse duration of about 20 fs. Typical transient transmission changes were about 1%.

The cross correlation and time zero were measured at the sample position by difference frequency generation in a 25-μm-thick BBO crystal yielding a cross correlation width of typically 35 fs (fwhm). To ensure the highest possible precision in the determination of time zero, cross correlations were recorded immediately before and after the molecular transients. Only if their width and temporal position agreed did we use the recorded trace for the evaluation. In this way, a precision for time zero of ± 5 fs was achieved.

Commercially available HBT was purified by recrystalization and dissolved in cyclohexane to a concentration of 6×10^{-3} M. A 70-μm-thick liquid jet of the solution served as the sample with an absorption at the pump-pulse wavelength of 50%.

The dependence of the transmission on the delay time in the pure solvent was also measured, and only at the very shortest probe wavelength, a small but significant signal was found. This

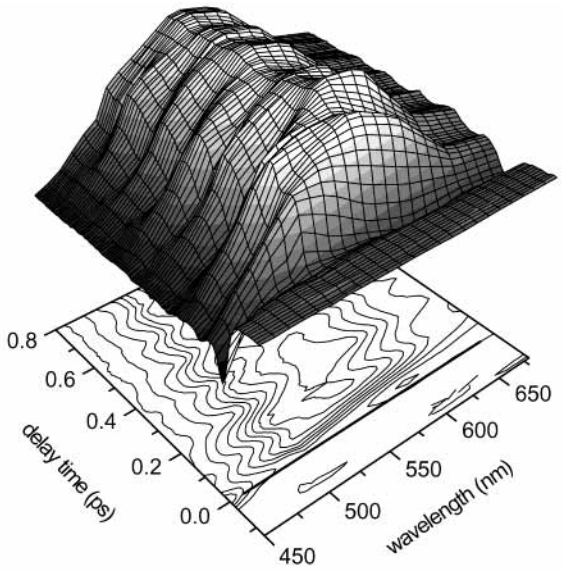

Figure 2. Change of the sample transmission as a function of both the central wavelengths of the probe pulses and the delay time between pump and probe pulses.

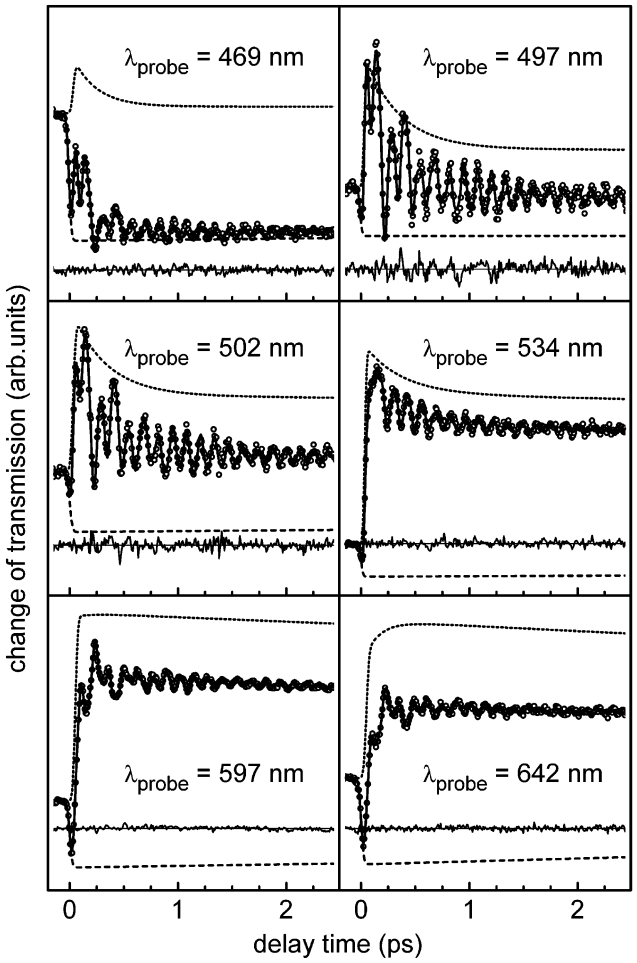

Figure 3. Experimental trace of the transmission change (○), fit (−), residual (thin line), and contribution of the excited-state absorption (- - -) and the nonoscillatory part of the emission (···) at six different probe wavelengths.

contribution depended linearly on the pump-pulse energy and was subtracted from the data. The results presented below were obtained with parallel polarization of the pump and probe pulses. Measurements with perpendicular polarization and at magic angle show that orientational relaxation occurs on a time scale of 50 ps and does not interfere with the dynamics due to the ESIPT.

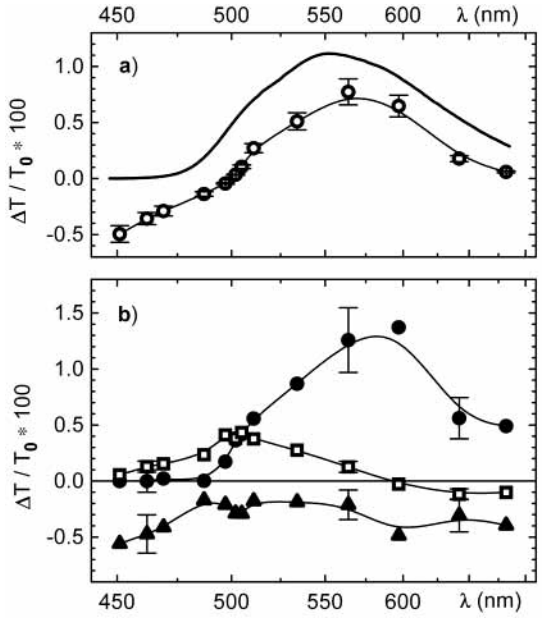

Figure 4. (a) Scaled CW fluorescence spectrum multiplied by λ^4 (−) and the transmission change $\Delta T/T_0$ at 3 ps (○). (b) Amplitudes of the short-lived (□) and the enduring (●) emission component and of the excited-state absorption (▲). The thin lines are guides for the eye.

III. Experimental Results and Data Analysis

HBT was excited at 347 nm, and the time-dependent transmission changes were measured at 13 wavelengths throughout the visible region. Figure 2 shows a pseudo-3D graph constructed from all experimental traces to facilitate an overview. A selected number of the traces are depicted in Figure 3 together with the results of the fitting procedure described below.

All traces show an initial decrease of the transmission at time zero followed by a delayed rise of the transmission and pronounced oscillation lasting for about 2 ps. The total transmission change is positive for probe wavelengths larger than 500 nm. In this spectral region, no ground-state bleaching signal can occur, and the transmission increase is solely due to stimulated emission from the keto-HBT, which is responsible for the fluorescence in the visible (Figure 1). After the oscillations have ceased, the transmission change stays practically constant for many tens of picoseconds. Its spectral dependence closely resembles the CW emission spectrum with a small offset (Figure 4a). This offset is due to excited-state absorption (ESA) from the S_1 state to higher electronic states that depends very weakly on the wavelength in the probed spectral range. ESA appears immediately after the molecules are excited and is responsible for the initial transmission decrease at time zero.

The subsequent rise of the transmission is caused by the stimulated emission originating from the keto form that emerged from the ESIPT as argued above. The delay of the transmission rise is therefore the time when the excited wave packet reaches the keto form. A visual inspection of the traces shows an ESIPT time between 35 fs at probe wavelengths in the blue spectral region and 60 fs in the red. A detailed analysis by means of a fitting procedure is given below.

Of great importance to the investigation of the reaction path are the pronounced and long-lasting signal oscillations. In Figure

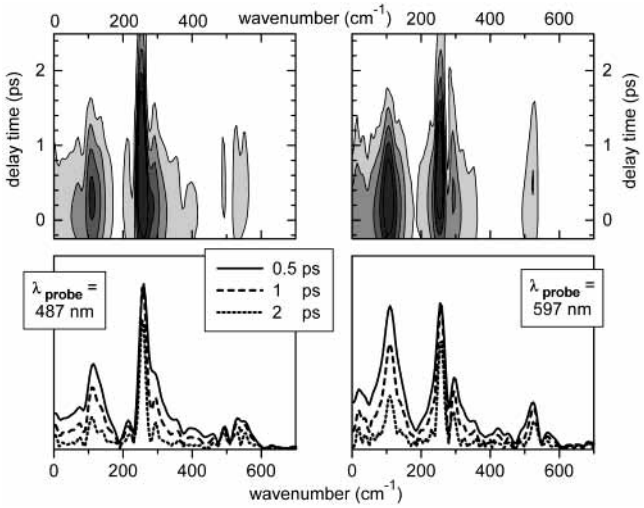

Figure 5. Sliding-window transformation of the experimental traces at probe center wavelengths 487 and 597 nm with a window width of 1 ps. The nonoscillatory signal contributions have been previously subtracted. The lower panels show the transformation results when the center of the time window is set to 0.5, 1, and 2 ps.

2, it can be clearly seen that the whole emission spectrum shifts periodically up and down in wavelength. Accordingly, the signal oscillations of the experimental traces in Figures 2 and 3 show a phase shift of π for probe wavelengths in the blue wing of the emission spectrum with respect to measurements in the red wing (compare also Figure 3 of ref 18). Figure 5 depicts sliding-window Fourier transformations and cuts of the transformations at some selected delay times for two exemplary traces, one in the blue wing of the CW emission spectrum at 487 nm and one in the red wing at 597 nm. Before the transformation, the nonoscillating components were subtracted, and a window function with a temporal width of 1 ps was used. Four frequency components contribute significantly to the oscillation pattern, one at about 110 cm^{-1}, the dominant one around 250 cm^{-1}, and two weaker ones at about 300 and 520 cm^{-1}. All of them are decaying on a picosecond time scale.

To extract the individual signal components in detail, every experimental trace was fitted with the following model function $S(t)$:

$$S(t) = \mathrm{CC}(t) \otimes \{S_{\mathrm{ESA}}(t) + S_{\mathrm{SE}}(t) + \sum_{i=1}^{4} S_{\mathrm{osc}}^{i}(t)\}$$

$$\approx \mathrm{CC}(t) \otimes \{A_{\mathrm{ESA}} \mathrm{e}^{-t/\tau_{\mathrm{slow}}} \cdot \Theta(t) + [A_{\mathrm{SE}}^{\mathrm{fast}} \mathrm{e}^{-[(t-t_{\mathrm{SE}})/\tau_{\mathrm{fast}}]} + A_{\mathrm{SE}}^{\mathrm{slow}} \mathrm{e}^{-[(t-t_{\mathrm{SE}})/\tau_{\mathrm{slow}}]}] \cdot \Theta(t - t_{\mathrm{SE}})\} + \sum_{i=1}^{4} A_i \cos(2\pi\nu_i t - \varphi_i) \mathrm{e}^{-[(t-t_{\mathrm{SE}})/\tau_i]} \cdot \Theta(t - t_{\mathrm{SE}})$$

The total transient signal is given by the sum of the molecular response functions $S_{\mathrm{ESA}}(t)$, $S_{\mathrm{SE}}(t)$, and $S_{\mathrm{osc}}(t)$ convoluted by the Gaussian cross correlation CC(t). The instantaneous excited-state absorption is taken into account by an exponential component with a negative amplitude A_{ESA} that decays with a time constant τ_{slow} on the order of 70 ps. This time constant accounts for orientational relaxation and internal conversion. The excited-state absorption sets in with a step at time zero modeled by the heavyside function $\Theta(t)$.

The nonoscillating part of the stimulated emission is delayed by t_{SE} (see discussion below) and consists of a fast component with amplitude $A_{\mathrm{SE}}^{\mathrm{fast}}$ and a decay time τ_{fast} of about 250 fs and a slow component with amplitude $A_{\mathrm{SE}}^{\mathrm{slow}}$ and the same decay time τ_{slow} as the transient absorption. The fast contribution accounts for the red shift of the emission spectrum; the slow one corresponds to the intensity of the CW emission spectrum. The convolution with the instrumental response function CC(t) can be expressed as a product with an appropriate error function that is easily evaluated during the iterative fitting procedure.

The four oscillating signal contributions are characterized by their frequencies ν_i, amplitudes A_i, phases φ_i, and damping times τ_i. According to Figure 2, the oscillating components are associated with the emission signal; therefore, their emergence is modeled by the same time shift t_{SE} as the emission. The convolution of the cos function with the Gaussian CC(t) can be evaluated only numerically, and this slows the fitting considerably. From a simulation, we found that the convolution hardly changes the shape of the cos function and reduces only the amplitude. We therefore omit the convolution for the oscillatory contribution. The results of the sliding-window transformation (see Figure 5 and the description above) were used as starting values for the fitting procedure.

In Figure 3, six experimental traces are depicted together with the fits and the contributions of the excited-state absorption and the nonoscillating part of the emission. The agreement between the fits and the experimental data is excellent (see residuals in Figure 3). Despite the large number of parameters, the fitting function uniquely resembles the important features of the excited-state dynamics. The independent fitting results of the individual traces nicely match, and their dependence on the probe wavelength strongly supports our model. This strongly supports the physical relevance of the chosen model function and the parameters.

The experimental traces recorded at the two shortest probe wavelengths of 451 and 462 nm cannot be satisfactorily fitted by the model function given above. At time zero, there is an additional Gaussian signal contribution that is particularly strong for the probe wavelength of 451 nm. An additional Gaussian absorption with the temporal width of the cross correlation yields a satisfactory fit. This contribution is believed to be due to nonlinear effects in the HBT solution. Because of the additional signal contribution, the two traces corresponding to wavelengths outside of the CW emission spectrum of HBT are not used in the global discussion of the proton-transfer dynamics.

IV. Interpretation of the Signal Components

In this section, the parameters resulting from the fitting procedure are presented, and their meaning with regard to the ESIPT process and their dependence on the probe wavelength are discussed. There are two groups of parameters. One describes the properties of the emerging keto form and contains the strength of the stimulated emission (SE) and the excited-state absorption (ESA) as well as the relaxation dynamics. The second group characterizes the oscillatory components and the features of the wave packet motion. A special role is played by the delay of the emission rise, which reveals the precise time of the ESIPT.

The description of the ultrafast ESIPT is a fully quantum mechanical problem. In the situation where the electronic configuration changes faster than the oscillation period of relevant normal modes, the proper description is a wave packet launched at the Franck−Condon point that propagates on the multidimensional excited-state PES. In the case that it keeps a small spatial extension (see section IV B), there is no appreciable difference between the quantum and classical descriptions of the particles (Ehrenfest's theorem). It is in this sense that we

understand our classical wording given below as a description of the quantum mechanical behavior.

A. Nonoscillatory Components. Let us first consider the nonoscillatory signal contributions that reflect the properties of the S_1 keto configuration. From the signal strengths at delay times when the oscillations are already damped out, the main contributions can readily be identified. In Figure 4a, the transmission change 3 ps after the excitation is compared to the CW fluorescence spectrum of HBT in cyclohexane. The error in the time-dependent signals stems from the uncertainty of the excitation intensity used for the individual measurements. The fluorescence spectrum is normalized and multiplied by λ^4 to convert the fluorescence probability to a measure of the wavelength dependent SE cross section.[35] The transient signal shows the same wavelength dependence as the scaled fluorescence apart from a small negative offset. This indicates that the signal is the sum of the SE from the S_1 keto state and a weak ESA with a flat wavelength dependence.

Because the ESA signal sets in at time zero within experimental accuracy, we have to associate it in the initial phase of the reaction with the enol configuration. Because of the flat wavelength dependence of the ESA from the keto configuration, we assume that the enol and the keto ESAs are quite similar and that the ESA spectrum is time-independent.

The amplitudes of the exponential components in the fit are shown in Figure 4b. These are the SE decaying in about 70 ps, the initial shift of the SE that gives rise to a 250-fs decay or rise of the signal depending on the probe wavelength and the transient ESA that decays with the same 70-ps time constant as the emission. Because both the SE and the ESA contribute with the same time constant to the signal after the first 100 fs, they correlate to some extent, leading to an error of about 0.001 in addition to the experimental uncertainties. Within this error, the amplitude of the enduring emission component follows the scaled CW fluorescence spectrum. This indicates that it characterizes the emission properties of the equilibrated keto form in the S_1 state that is responsible for the CW fluorescence.[11,33] The amplitude of the excited-state absorption is fairly constant over the investigated wavelength region. Ernsting and co-workers showed that in the case of 2,5-bis(2′-benzoxazolyl)-hydroquinone the excited-state absorption has a very strong band at about 530 nm but is 8 times smaller and shows only a weak wavelength dependence for wavelengths larger than 580 nm.[36] Ongoing experiments with other ESIPT systems in our group indicate that the spectral position of the strong excited-state absorption band varies strongly with the molecule. The corresponding excited-state absorption band of HBT is obviously located at shorter wavelengths, and the used probe pulses sample the weaker and only slightly varying absorption to the red of it.

The additional component with a time constant of about 250 fs has a positive amplitude for probe wavelengths below 580 nm and a negative one for shorter wavelengths. Its magnitude correlates roughly with the slope of the scaled CW fluorescence spectrum, and the change in sign is the manifestation of the change from signal decay to rise (compare Figure 3). Overall, this component describes a red shift of the SE spectrum, which we interpret as the signature of internal vibrational redistribution (i.e., the geometrical relaxation that also causes the dynamic Stokes shift[32]).

In Figure 6, the time constants of the red shift and the overall signal decay are depicted as a function of the probe wavelength. They show a significant but smooth variation. If the underlying dynamics can be described by the appearance of one species and the disappearance of another, then the time constants should be independent of the probe wavelength. Changes in the spectral shape due to vibrational redistribution and cooling have a more complex time dependence than a uniform exponential change and lead to fitted time constants that vary with the probe wavelength.[5,37]

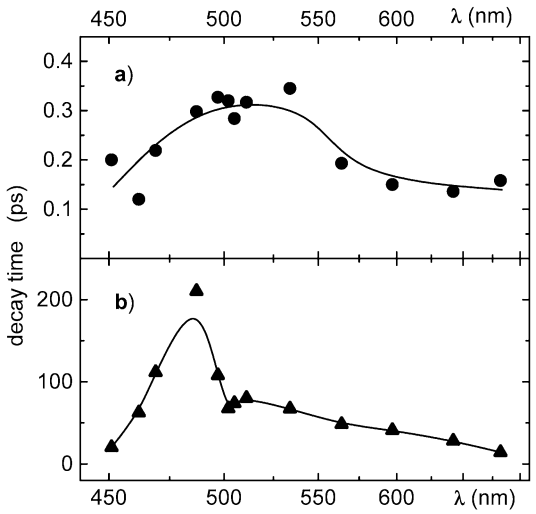

Figure 6. Time constant of the short-lived emission component (●, panel a) and of the overall signal decay (▲, panel b) as a function of the probe wavelength. The lines are guides for the eye.

The time constant associated with the spectral red shift is around 250 fs (Figure 6a) and is fairly short for complete IVR. That IVR has some components occurring on this time scale was also observed for dye molecules.[38] The electronic rearrangement associated with the ESIPT process affects a few modes strongly but to some degree all of them. The reaction to these changes is evidenced in the ultrafast dynamic Stokes shift. However, only a small part of the vibrational energy is redistributed by this process, as will be evident in the following.

The time constant describing the long-time behavior of the signal adopts values between 14 and 200 ps. The situation is rather complex because a lot of processes contribute to the decay. The slowest one should be the internal conversion to the electronic ground state occurring on a time scale of several hundred picoseconds.[11,33] Measurements with parallel and perpendicular polarization reveal a time scale of 50 ps for the orientational relaxation (see above). Ongoing IVR and vibrational cooling due to contact with the solvent seem to change the spectral shape and contribute to the long-time constant too. The cooling is best seen in the more rapid decays in the spectral wings and in good quantitative agreement with the 15-ps time constant reported recently.[21] To some extent, the excited-state absorption might also show spectral reshaping. Depending on the probe wavelength, the contribution of theses processes to the transmission signal can be opposing, leading to a slower change, or constructive, causing accelerated signal decay. Because all of this happens after the actual ESIPT and does not interfere with it, no further investigations were carried out to differentiate the contributions to the slow signal decay.

B. Delayed Rise of Emission. A rise of the sample transmission is observed with a small but finite delay after the excitation. In Figure 7a, the temporal region around time zero is shown in more detail for selected experimental traces. Visual inspection reveals that for probe wavelengths below 550 nm (i.e., in the blue wing of the emission spectrum) the delay is 35 fs and for wavelengths in the red wing it is 60 fs. The fitting procedure results in values of the delay (Figure 7b) that are somewhat

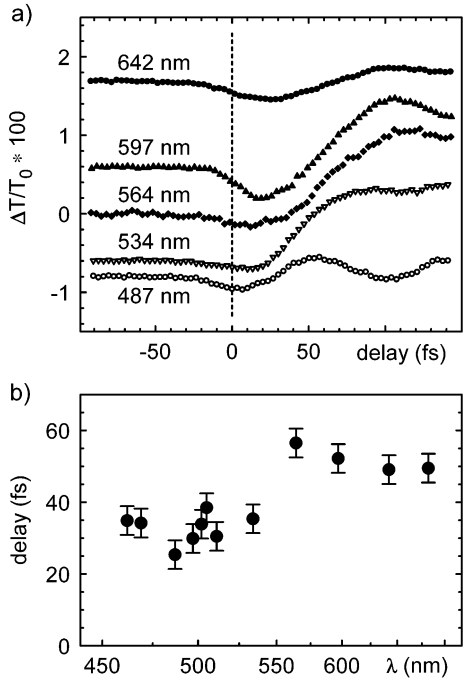

Figure 7. (a) Experimental traces around time zero showing the delayed rise of the emission. (b) Fitted delay of the steplike emission rise as a function of the probe wavelength.

shorter because it takes the ESA into account, which masks the initial part of the rise. The values form two groups with very little variation within. For probe wavelengths below 550 nm, the time delays cluster around a mean value of 33 fs, and above 550 nm, the time delays cluster around a mean value of 52 fs.

The rise of the transmission can safely be associated with the appearance of the keto form. Thus, after 33 fs the molecule adopts for the first time a keto configuration and can emit in the visible, but it is still displaced with respect to the keto minimum (i.e., the equilibrium geometry of the keto form). Because the S_1 and S_0 potential energy surfaces come closer to each other along the reaction coordinate, regions of the S_1 surface showing blue emission are reached by the wave packet prior to regions with red emission, and it takes another 20 fs until the wave packet also samples the red emitting regions.

Further insight can be gained by a precise analysis of the transmission rise. The experimental trace at 564 nm with rather weak oscillatory signal components is selected for this purpose. Figure 8a shows a fit with a pure exponential increase (broken line) and the exponential increase convoluted with the cross correlation (solid line). In Figure 8c, the experimental trace is fitted by a delayed step function (broken line; with convolution, solid line). For comparison, Figure 8b shows the sum of the instantaneous excited-state absorption and the delayed, steplike increasing emission convoluted with the cross correlation (broken line) as well as the complete fit including the oscillations (solid line). The fitted exponential increase and the delayed, steplike model yield the same time scale of 60 to 70 fs for the rise of the emission. The inclusion of the excited-state absorption and the oscillatory signal components results in a reduction of this time by 10 fs. Despite the correct time scale, the exponential increase shows much stronger deviations from the experimental trace during the first 150 fs. Particularly, it is not able to model the steep rise of the transmission increase. The delayed step model, however, matches the experimental data very well and catches the main features of the curve.

An exponential time dependence is expected if the relevant process can be characterized by the depopulation of one state

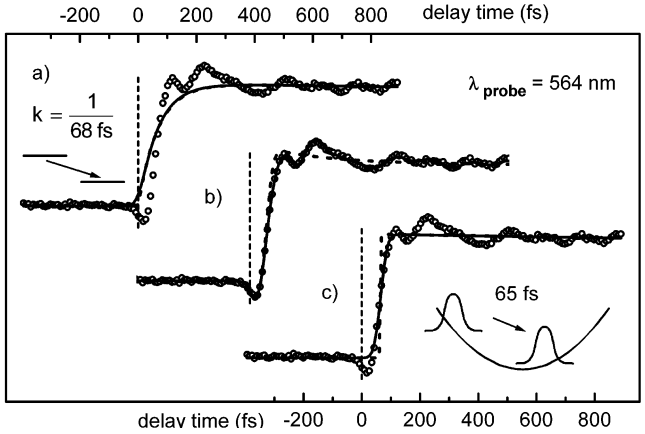

Figure 8. Experimental trace at 564 nm fitted by various model functions. (a) Pure exponential increase (- - -) and exponential increase convoluted with cross correlation (−). (b) Sum of the fitted instantaneous excited-state absorption and the delayed, steplike increasing emission convoluted with the cross correlation (- - -) as well as the complete fit including the oscillations (−). (c) Pure step function shifted with respect to time zero (- - -) and the same function convoluted with the cross correlation (−).

and the corresponding population of other states via a rate-governed process. This situation exists, for instance, if there is a comparatively weak coupling between the two states and Fermi's Golden Rule can be adopted[39] or if the system has to cross a significant energy barrier to arrive at the second state.[40] Tunneling of the proton through an energy barrier would also lead to an exponential signal change because the frequency of hydrogen vibrations is so high that it is not even possible to resolve it with our superior time resolution and only a temporally averaged transition rate should appear in the experiment.

In contrast, a steplike signal change indicates that the system reaches the detection window at a well-defined time and not gradually. In terms of wave packet dynamics, this means that a wave packet enters the region of the configuration space, which is observed by the detection process, within a short time interval. Therefore, the wave packet has to be rather confined, and the process can be characterized as a movement of the complete wave packet without pronounced spreading. By analogy to the nonstatistical movement of a classical particle, we call this a ballistic wave packet motion. The experimentally observed time delay is the interval between the time that the wave packet is launched in the Franck−Condon region and the time that the wave packet reaches the region where the detection process is sensitive. A delayed signal rise due to such a coherent unhindered wave packet motion was also observed by A. Zewail and co-workers for direct dissociation processes[41,42] and by W. Fuss et al. for the dynamics after an internal conversion through a conical intersection in the case of 1,3-cyclohexadiene.[43]

According to Figures 3 and 8, the experimental traces can be well fitted by a delayed steplike emission rise but only unsatisfactorily by an exponential increase. Because the emission rise is due to the appearance of the keto form (see above), we conclude that the ESIPT of HBT happens in the form of a ballistic wave packet motion. This implies that the tunneling of the proton is not the relevant mechanism in the description of the process.

C. Oscillatory Components Induced by the ESIPT. In Figure 9a, the fit results are depicted for the frequencies of the four oscillations included in the model function, which also show up in the sliding-window transformations (Figure 5). They are numbered with increasing frequency from 1 to 4. Oscillations 1 and 2 with frequencies of 113 and 255 cm^{-1}, respectively,

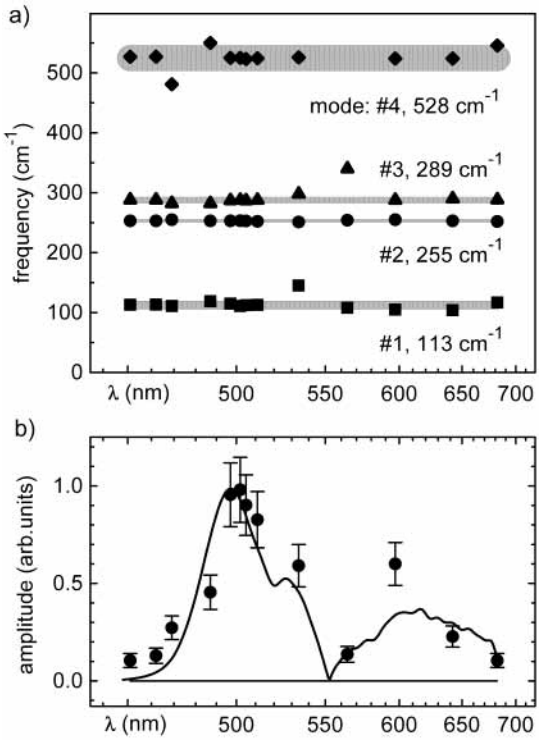

Figure 9. (a) Frequencies of the fitted oscillations. The vibrational modes are numbered with increasing frequency. (b) Slope of the scaled fluorescence spectrum (−) and amplitude of the dominant oscillation (mode 2, 255 cm^{-1}; ●) as a function of the probe wavelength.

are quite strong; 1 decays with a time constant of about 300 fs, and 2 decays with a time constant of 1 ps. Because of its large amplitude and long decay time, oscillation 2 at 255 cm^{-1} is the dominant oscillatory contribution and is responsible for the characteristic shape of the experimental traces. The other two oscillations, 3 and 4 at 289 and 528 cm^{-1}, respectively, decay with time constants of somewhat less than a picosecond and are much less pronounced. These results are almost independent of the probe wavelength, confirming that the same kind of oscillations can be seen in all traces. Only the experimental trace at a probe wavelength of 564 nm near the maximum of the emission spectrum does not show weak oscillation 4, and the measurements at 469, 462, and 451 nm, which are at or already beyond the blue edge of the CW fluorescence spectrum, exhibit an accelerated damping of the oscillations because the red shift moves the emission out of the detection windows.

The damping times of the oscillations are in excellent agreement with the 700-fs relaxation time found in recent IR measurements.[21] They can be safely attributed to the solvent-assisted IVR.

Because of our cross-correlation width of 35 fs, signal oscillations with a frequency well above 700 cm^{-1} can hardly be detected. Therefore, we cannot tell directly from the time-resolved data whether high-frequency modes are excited. We can, however, exclude a significant excitation of these modes by considering the amount of vibrational energy that is released by the ESIPT. In the case of 2-(2′-hydroxyphenyl)benzoxazole, which is very similar to HBT but has an accidental degeneracy of the enol and the keto triplet states, Nickel and co-workers found that in the ground state the keto form is 4900 cm^{-1} above the stable enol form whereas in the electronically excited state the keto form is 2100 cm^{-1} below the enol form,[44,45] In other words, only about one-third of the observed Stokes shift is due to the potential energy decrease in the S_1 state on going from the enol to the keto form, and the rest results from the energy increase in the ground state. This seems to be a general feature of molecules exhibiting ESIPT. For example, ab initio calculations on *o*-hydroxybenzaldehyde indicate that the keto minimum in the S_1 state lies 2400 cm^{-1} below the Franck−Condon point whereas the S_0 state shows an energy increase of 5100 cm^{-1} in the keto form.[27] These calculations are in good agreement with recent time-resolved photoelectron measurements.[14] In the case of HBT, the Stokes shift between the absorption and emission onsets amounts to 7500 cm^{-1} according to Figure 2 and ref 16; therefore, potential energy of about 2500 cm^{-1} should be released by the ESIPT. This estimate is in excellent agreement with the ab inito calculations reported in the accompanying paper.[29] Spectra of HBT crystals exhibit a quite similar Stokes shift and a comparable energy release by the ESIPT.[46] Because each of the four vibrational modes that are responsible for the oscillatory signal contributions has to contain quite a bit of energy, there is not enough left to excite other modes significantly. For example, if one assumes that the two dominant modes are excited by five quanta and that the two weak modes are excited by one quantum then the total energy in these four modes adds up to 2657 cm^{-1}. In particular, the excitation of local OH and NH modes with their high frequencies can be excluded. Interestingly, very recent time-resolved IR measurements nicely proved this point in an elegant and direct way.[21]

In Figure 9b, the spectral dependence of the amplitude of dominant oscillation 2 is compared to the first derivative of the CW emission spectrum. The excellent correlation is in full agreement with the impression gained from Figure 2 that the oscillations are caused by an oscillatory spectral shift of the entire emission spectrum. At a given probe wavelength, the periodic shift translates into a periodic transmission change that is proportional to the slope of the spectrum and is closely related to the displacement between the keto S_1 and S_0 normal modes as well as the keto transition cross section. Accordingly, the oscillatory signal pattern is suppressed near the maximum of the emission spectrum, explaining the weakness of the oscillations at 564 nm. The oscillatory spectral shift also leads to a phase jump of π at probe wavelengths around 550 nm, which can be seen for the dominant oscillation and is confirmed by the fitting procedure for all oscillations.

Because the oscillatory signal components mirror the periodic shift of the keto emission spectrum, they have to be caused by oscillations in vibrational coordinates of the S_1 keto form (i.e., the product of the ESIPT). Therefore, the fitted frequencies are the eigenfrequencies of the normal modes of the S_1 keto form, which are hardly detectable by other spectroscopic methods. Because of the large Stokes shift, it can be excluded that a wave packet excited by impulsive Raman scattering in the electronic ground state contributes to the signal.

According to Figure 1, the optical excitation is less than 1000 cm^{-1} above the hypothetical enol origin, and the energy release due to the ESIPT is expected to be on the order of 2500 cm^{-1} (see discussion above). Because the major part of the vibrational energy that is finally available is released by the ESIPT and the vibrational excitation is coherent, we conclude that the observed coherent oscillations in the product state are mainly excited by the ESIPT itself and not by the optical excitation. It is interesting to compare the present observations to the resonance Raman spectrum. The optical excitation of vibrational modes is directly connected to the slope of the excited-state PES at the Franck−Condon point that leads to an accelerated motion of the wave packet out of the Franck−Condon region.[47] The relative intensities of the fundamentals in the resonance Raman spectrum are a measure of the contributions of the

particular modes to the potential slope. Extensive resonance Raman studies were performed on HBT and related compounds,[48,49] and it was found that the ground-state modes at 118, 266, 293, and 537 cm^{-1} that correspond to the excited-state vibrations observed by us carry reasonable Raman intensity. A direct comparison of the intensities to the oscillation amplitudes found by us is not possible because different transition cross sections are relevant. In addition, the resonance Raman spectrum shows even stronger lines at frequencies around 1500 cm^{-1}. As argued above and shown in the IR measurements, these modes are not excited after the ESIPT.[21] It seems that one cannot deduce from a resonance Raman spectrum the vibrational excitation by a process during which the wave packet evolves far beyond the Franck−Condon region. The reaction path of the ESIPT in HBT must be strongly curved, and the projections of vibrational modes on the reaction path can change dramatically during the course of the reaction. The very first part of the reaction path has projections on modes around 1500 cm^{-1} because the optical excitation is accompanied by immediate changes in the electronic density leading to changes in bond lengths and in the corresponding stretching coordinates. These modes are likely to dominate the resonance Raman spectrum. But after the Franck−Condon region, the ESIPT reaction path is dominated by low-frequency modes, leading to their coherent excitation and thereby to the observed signal oscillations. (See also the accompanying work.[29])

It is worth noting that a well-defined wave packet is created by the ESIPT process that survives for a time on the order of a picosecond despite the reactive PES and the influence of the solvent. The wave packet exhibits a strong localization because its dynamics is restricted to only 4 modes out of 69 nuclear degrees of freedom. The implications of such a localization on the dynamics and the functionality are discussed elsewhere.[32] Here we state only that the IVR of HBT is comparable to that of nonreactive molecules[38,50] and that even 1 ps after the excitation the molecule is far from behaving statistically.

D. Role of Skeletal Vibrations. Further insight into the ESIPT process can be gained by analyzing the nuclear motions associated with the vibrational modes that are selectively excited by the ESIPT. Ab initio calculations were performed to identify the four modes appearing in the time-resolved data.[29] The ground state was computed using density functional theory (DFT) and the S_1 state by time-dependent DFT. In both cases, the B3LYP functional and the 6-31G* basis set were applied. Details of the methods and the complete results will be presented in the accompanying paper.[29] Here we refer only to some findings that are important to the present discussion. For the electronic ground state, four vibrational eigenmodes are found with frequencies similar to our data. The calculated frequencies of 118, 278, 323, and 553 cm^{-1} agree well with other theoretical results and the resonance Raman spectra.[48,49] According to the calculations, nearly the same modes are also eigenmodes in the keto minimum of the S_1 state. The computed frequencies of 116, 258, 288, and 514 cm^{-1} agree excellently with our experimental results, and we conclude that the ab initio calculations also reproduce the nuclear motions that are responsible for the oscillatory signal contributions.

These nuclear motions associated with the four relevant normal modes are depicted in Figure 10. Mode 1 (corresponding to oscillation 1) is an in-plane bending of the entire molecule, and mode 2, which dominates the experimental traces, corresponds to a stretching of the molecule. Modes 3 and 4 can be described as rotations of the ring moieties. All four modes strongly deform the central H-chelate ring and modulate the

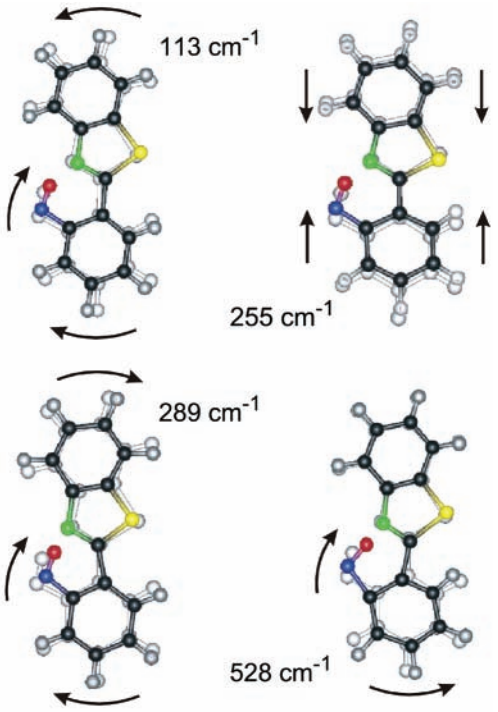

Figure 10. Calculated vibrational motions of the modes observed in the experiment.

distance between the oxygen and the hydrogen-accepting nitrogen whereas the geometry of the phenyl rings is barely affected.

Why are these modes especially excited by the ESIPT? Let us consider an intuitive excitation mechanism that can explain most of the experimental findings. When a chemical reaction takes place, at least a few bonds and their strength are strongly changed. This leads to a new equilibrium geometry of the molecule that is the product form. If this happens very quickly, then the nuclei cannot follow because of their inertia, and directly after the reaction the molecule is displaced with respect to the new equilibrium, which is quite analogous to an optical Franck−Condon transition. Therefore, the nuclei start to oscillate around the new equilibrium geometry (i.e., the potential minimum of the product form). This leads to a coherent excitation of those vibrational eigenmodes of the product that involve bonds that have changed and the molecule "rings" in coordinates affected by the reaction. By identifying these modes and their nuclear displacements, we can localize the changes induced by the reaction and reconstruct the reaction path.

A change of bonds is first of all an electronic configuration change (i.e., some electrons have to switch the orbitals they occupy). Because of the small electron mass, this can proceed in a very short time in comparison to the time required for nuclear motions. The condition is that the change of the electronic configuration happens at a rather well-defined molecular geometry (i.e., within a small area of the PES). Otherwise, the electronic configuration would vary gradually along the nuclear coordinates, and the time scale of the electronic change would be given by the nuclear motion. The Born−Oppenheimer approximation is violated in this initial phase of the ESIPT. However, the wave packet still evolves along a single adiabatic PES.

According to the proposed mechanism, the molecule will start to oscillate in the newly defined normal modes when it changes its electronic configuration. The beginning of the oscillation is encoded in the phases that are obtained by the fitting procedure

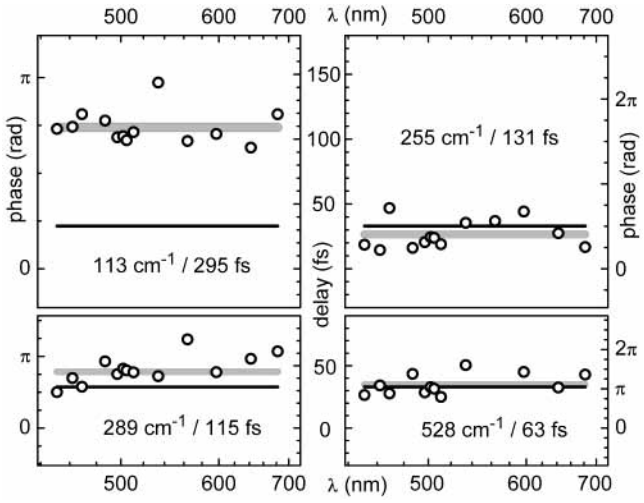

Figure 11. Probe wavelength dependence of the phase (outer scales) and the turning time of the four vibrations (inner scales) as determined from the fitting procedure. The frequency and the period of each vibration are shown for convenience. The gray bars indicate the time intervals of $\pm 1\sigma$ of the mean values, and the black lines are drawn at 33 fs corresponding to the appearance of the keto form.

(Figure 11). For a coherent vibronic excitation caused by the optical excitation at resonance, the phase is expected to be 0 or π.[51] Clearly, for the three lower-frequency modes this is not found. For the highest-frequency mode, half of the period closely matches the 33-fs ballistic delay; therefore, this mode cannot contribute to the decision of whether the mode excitation is mainly due to the optical transition or the ESIPT.

A more instructive picture emerges when we calculate from the phase and the frequency for each oscillation the point in time when the molecule is for the first time at a turning point of this vibration. This corresponds to the maximum displacement and the start of the oscillation. The results are shown in Figure 11 as a function of the probe wavelength. The gray bars indicate the time intervals of $\pm 1\sigma$ of the mean values, and the black line is drawn at 33 fs when the keto configuration is adopted for the first time.

For the three vibrations with the higher frequencies (i.e., modes 2 to 4), the turning point is adopted at times near the appearance of the keto form, indicating that these vibrations are indeed mainly excited by the proposed mechanism (i.e., by a fast change from the enol to the keto configuration 30 to 35 fs after the optical excitation). However, the bending vibration (mode 1) approaches its turning point roughly a quarter of a period after the electronic configuration change. Obviously, the molecule gains considerable momentum along this coordinate before the electronic switching. This implies that the first part of the reaction path, which leads to the configuration change, is dominated by this motion and that the slope of the potential surface is initially mainly oriented along its direction.

V. Conclusions: Sequence of ESIPT

The new experimental data and the preceding analysis allow us to deduce a novel model for the ESIPT that is schematically depicted in Figure 12. It accounts well for the duration of the ballistic wave packet motion and the observed coherent vibrations. As discussed above, the ballistic wave packet motion, which is a direct process and not slowed by a barrier or tunneling probability, takes about 33 fs to enter the area of the PES belonging to the keto configuration. If the degrees of freedom, which have to change significantly during the ESIPT, are the position of the proton or are purely electronic, then one would

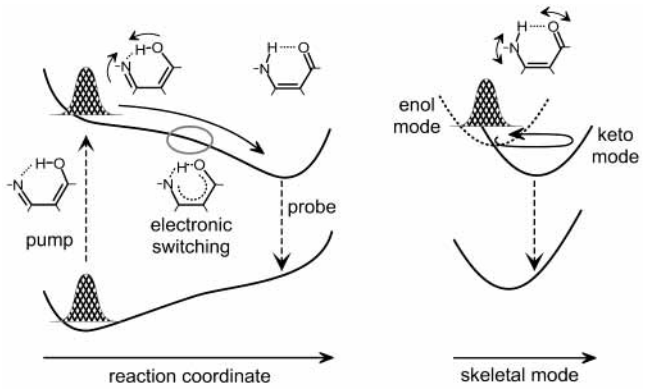

Figure 12. Schematic potential energy surface and wave packet motion according to the ESIPT model along the reaction coordinate (left) and a skeletal mode (right) that is excited by the electronic configuration change. Sketches of the chelate ring denote the steps of the ESIPT. For details, see the text.

expect a time of less than 10 fs[12] because of the small mass of the participating particles. The reason for the longer time is that the initial motion involves extended skeletal motion and therefore a number of heavier nuclei. Their inertia determine the time of the ESIPT process.

The participating skeletal modes have been identified above. They are in-plane deformations of the H-chelate ring and lead to a large variation of the ON distance (i.e., the distance between the oxygen of the enol group and the hydrogen-accepting nitrogen). A reduction of the ON distance favors the formation of the NH bond and therefore induces the electronic configuration change. It was previously proposed that low-frequency large-amplitude motions determine the transfer time,[11] and very specifically it was argued that in the case of HBO the transfer rate is given by the frequency of the in-plane bending vibration[13] because this vibration modulates the ON distance and thereby the barrier between the enol and keto forms. This model was later extended to rationalize the ESIPT of 2-(2′-hydroxyphenyl)-5-phenyloxazole.[7,52] In the case of TINUVIN P, the coherent excitation of a vibration was observed that acts as a geared in-plane rotation of two subunits against each other corresponding to mode 3 of HBT, and this motion was assigned to the modulation of the ON distance.[17] All of these considerations introduce the modulation of the high-frequency proton coordinate by a low-frequency skeletal mode.

As discussed above, we deduce from the phases of the oscillations that mode 1 (i.e., the bending motion of the entire molecule) dominates the first part of the reaction path. The initial contraction of the H-chelate ring and the reduction of the ON distance are therefore mainly caused by the in-plane bending of the molecule. However, when the ON distance has shortened to a critical value roughly 33 fs after the optical excitation, the electronic configuration changes in an extremely short time. By this "electronic switching" the hydrogen gets bonded to the nitrogen, the single and double bonds of the chelate ring exchange their positions, and the molecule adopts its electronic keto configuration. The proton initially moves together with the oxygen, and after the configuration change it moves together with the nitrogen. At the moment of the "electronic switching" the molecule is geometrically displaced with respect to the potential minimum of the keto form. This leads to the coherent excitation of the other three modes, however not to the explicit motion of the proton. Because it takes some extra time until the wave packet passes through the minimum, the emission in the red spectral region is further delayed by about 20 fs. Contrary to the earlier ideas, the whole process is truly multidimensional

even with respect to the nuclear coordinates and intimately links electronic and nuclear motion.

Recent theoretical calculations on various ESIPT molecules support this picture[22−25,30] because they find a significant shortening of the distance between the proton donor and the acceptor atom halfway along the reaction path. The electronic configuration change manifests itself in the difficulty in calculating an accurate PES in the transition region. Therefore, the results on a possible potential barrier along the reaction path vary strongly with the applied method.[27,28] Nevertheless, the calculations indicate that the molecular skeleton is indeed bent in the transition region.[29] A direct comparison with time-resolved experiments is not yet possible because it is not clear whether the molecule enters the keto region of the PES at the transition region with the lowest possible energy or at a different geometry due to momentum conservation. A quantum dynamic calculation of the multidimensional wave packet motion is necessary to clarify this point.

In a 1D picture, the ESIPT would be reversible because the wave packet would be reflected at the back of the keto potential and would subsequently return to the enol form. In the multidimensional situation, the wave packet has to come back to the point of the PES where the "electronic switching" takes place. Because the wave packet is oscillating in four modes with different frequencies, it takes much more time until all vibrational motions rephase to reach this point again. Although a well-defined wave packet exists for a time on the order of a picosecond and internal vibrational redistribution is far from complete within the first several hundred femtoseconds, the process is nevertheless irreversible.

The proton itself behaves in a very passive way and changes its binding site adiabatically. The initial contraction of the chelate ring shifts the proton together with the oxygen toward the nitrogen. The change in the electronic wave function redistributes electronic density from the OH to the NH site and establishes the NH bond. The subsequent motion of the chelate ring toward its potential minimum pulls the proton together with the nitrogen away from the oxygen. In other words, the proton always stays in its local potential well that is shifted by the motions of the chelate ring. This is in agreement with the fact that there is by far not enough energy available to excite a local OH or NH vibration. The proton position is not a good choice for the reaction coordinate. The O−N distance is more closely related to the reaction coordinate. A correct choice has to be multidimensional, as discussed in detail in the accompanying paper, and might be given by the minimum-energy path from the Franck−Condon point to the keto minimum of the PES.

VI. Summary

In the work presented, we have applied pump−probe spectroscopy with a time resolution of 30 fs to the ESIPT of HBT dissolved in cyclohexane. From the delayed steplike rise of the emission, we conclude that the ESIPT proceeds as a ballistic wave packet motion. About 33 fs after the excitation, the molecule adopts the electronic keto configuration, and about 20 fs later, it approaches the potential minimum of the keto form. The transfer time is due to the inertia of the involved skeletal motions and is not due to a limited tunneling probability or the transition rate over a barrier. The time-dependent transmission shows strong oscillations that are damped on a picosecond time scale. This indicates that a well-defined wave packet is created and survives for that time despite the reactive PES and the influence of the solvent. Its dynamics is restricted to 4 skeletal modes out of 69 nuclear degrees of freedom. These modes are an in-plane deformation of the H-chelate ring and all modulate the ON distance. A significant excitation of any high-frequency mode can be excluded by energy arguments. The phases of the oscillations indicate that an initial bending of the entire molecule leads to a contraction of the H-chelate ring and induces the electronic configuration change. By the rearrangement of the electrons, new bonds are established; these are associated with a new equilibrium geometry, which is the keto minimum of the PES. The molecule is still displaced with respect to this equilibrium geometry along three additional skeletal coordinates, giving rise to coherent oscillations in these modes. The role of the proton is a passive one because it is shifted toward the nitrogen by the bending of the molecule, and the change of the bond is a result of the electronic switching. Contrary to previous models, we argue that the dynamics of the ESIPT is entirely governed by the evolution of the wave packet along several skeletal coordinates and that the hydrogen position follows all changes in an adiabatic fashion.

Only the lowest-frequency mode that comprises an overall bending of the molecular skeleton can initially be considered to be a promoting mode for the ESIPT process. The other three act as accepting modes. The coherent motion in these modes is the ringing of the product molecule along those coordinates that were heavily deformed by the electronic configuration changes of the ESIPT. We expect that similarly strong wave packet motions will be present in most unimolecular photoinitiated reactions because they all involve significant changes in the molecular geometries. The experimental observation of the corresponding signal oscillations in pump−probe measurements of the highest temporal resolution and with properly selected wavelengths will allow the identification of the vibrational modes involved. In combination with quantum chemical calculations, this will lead to an elucidation of the underlying reaction mechanism with unprecedented precision.

Acknowledgment. We thank Johannes Piel and Jörg Krebs for valuable experimental assistance, Peter Härter for help with the sample purification, and Regina de Vivie-Riedle, Vincent De Waele, and Wolfgang Domcke for many beneficial discussions. We also gratefully acknowledge continuous support by Wolfgang Zinth and financial support by the Deutsche Forschungs Gemeinschaft.

References and Notes

(1) For a review see: Barbara, P. F.; Trommsdorff, H. P., Eds.; *Chem. Phys.* **1989**, *136*, 153−360. All papers in this special issue are relevant.
(2) Ormson, S. M.; Brown, R. G. *Prog. React. Kinet.* **1994**, *19*, 45.
(3) Le Gourrierec, D.; Ormson, S. M.; Brown, R. G. *Prog. React. Kinet.* **1994**, *19*, 211.
(4) For a review see: Limbach, H.-H.; Manz, J.; Eds.; *Ber. Bunsges. Phys. Chem.* **1998**, *102*, 28−592. All papers in this special issue are relevant.
(5) Elsaesser, T. In *Femtosecond Chemistry*; Manz, J., Wöste, L., Eds.; VCH-Verlag: Weinheim, Germany, 1995; Vol. 2, pp 563−579.
(6) Barbara, P. F.; Walsh, P. K.; Brus, L. E. *J. Phys. Chem.* **1989**, *93*, 29.
(7) Douhal, A.; Lahmani, F.; Zewail, A. H. *Chem. Phys.* **1996**, *207*, 477.
(8) Weller, A. *Z. Elektrochem.* **1956**, *60*, 1144.
(9) Huston, A. L.; Scott, G. W.; Gupta, A. *J. Chem. Phys.* **1982**, *76*, 4978.
(10) Elsaesser, T.; Kaiser, W. *Chem. Phys. Lett.* **1986**, *128*, 231.
(11) Laermer, F.; Elsaesser, T.; Kaiser, W. *Chem. Phys. Lett.* **1988**, *148*, 119.
(12) Herek, J. L.; Pedersen, S.; Bañares, L.; Zewail, A. H. *J. Chem. Phys.* **1992**, *97*, 9046.
(13) Arthen-Engeland, Th.; Bultmann, T.; Ernsting, N. P.; Rodriguez, M. A.; Thiel, W. *Chem. Phys.* **1992**, *163*, 43.
(14) Lochbrunner, S.; Schultz, T.; Schmitt, M.; Shaffer, J. P.; Zgierski, M. Z.; Stolow, A. *J. Chem. Phys.* **2001**, *114*, 2519.
(15) Frey, W.; Laermer, F.; Elsaesser, T. *J. Phys. Chem.* **1991**, *95*, 10391.

(16) Ding, K.; Courtney, S. J.; Strandjord, A. J.; Flom, S.; Friedrich, D.; Barbara, P. F. *J. Phys. Chem.* **1983**, *87*, 1184.
(17) Chudoba, C.; Riedle, E.; Pfeiffer, M.; Elsaesser, T. *Chem. Phys. Lett.* **1996**, *263*, 622.
(18) Lochbrunner, S.; Wurzer, A. J.; Riedle, E. *J. Chem. Phys.* **2000**, *112*, 10699.
(19) Jethwa, J.; Ouw, D.; Winkler, K.; Hartmann, N.; Vöhringer, P. *Z. Phys. Chem.* **2000**, *214*, 1367.
(20) Ernsting, N. P.; Kovalenko, S. A.; Senyushkina, T.; Saam, J.; Farztdinov, V. *J. Phys. Chem. A* **2001**, *105*, 3443.
(21) Rini, M.; Kummrow, A.; Dreyer, J.; Nibbering, E. T. J.; Elsaesser, T. *Faraday Discuss.* **2002**, *122*, 27. Rini, M.; Dreyer, J.; Nibbering, E. T. J.; Elsaesser, T. *Chem. Phys. Lett.* **2003**, *374*, 13.
(22) Sobolewski, A. L.; Domcke, W. In *The Reaction Path in Chemistry: Current Approaches and Perspectives;* Heidrich, D., Ed.; Kluwer Academic Publishers: Dordrecht, The Netherlands, 1995; p 257.
(23) Rios, M. A.; Rios, M. C. *J. Phys. Chem.* **1995**, *99*, 12456.
(24) Jaworski, A. *Comput. Chem.* **1998**, *22*, 13.
(25) Rios, M. A.; Rios, M. C. *J. Phys. Chem. A* **1998**, *102*, 1560.
(26) Forés, M.; Duran, M.; Solà, M.; Adamowicz, L. *J. Phys. Chem. A* **1999**, *103*, 4413.
(27) Sobolewski, A. L.; Domcke, W. *Phys. Chem. Chem. Phys.* **1999**, *1*, 3065.
(28) Scheiner, S. *J. Phys. Chem. A* **2000**, *104*, 5898.
(29) de Vivie-Riedle, R.; De Waele, V.; Kurtz, L.; Riedle, E. *J. Phys. Chem. A* **2003**, *107*, 10591.
(30) Sobolewski, A. L.; Domcke, W. *Chem. Phys.* **1998**, *232*, 257.
(31) Riedle, E.; Beutter, M.; Lochbrunner, S.; Piel, J.; Schenkl, S.; Spörlein, S.; Zinth, W. *Appl. Phys. B* **2000**, *71*, 457.
(32) Wurzer, A. J.; Lochbrunner, S.; Riedle, E. *Appl. Phys. B* **2000**, *71*, 405.
(33) Barbara, P. F.; Brus, L. E.; Rentzepis, P. M. *J. Am. Chem. Soc.* **1980**, *102*, 5631.
(34) Wilhelm, T.; Piel, J.; Riedle, E. *Opt. Lett.* **1997**, *22*, 1494.
(35) Deshpande, A. V.; Beidoun, A.; Penzkofer, A.; Wagenblast, G. *Chem. Phys.* **1990**, *142*, 123.
(36) Ernsting, N. P.; Kovalenko, S. A.; Senyushkina, T.; Saam, J.; Farztdinov, V. *J. Phys. Chem. A* **2001**, *105*, 3443.
(37) Lochbrunner, S.; Fuss, W.; Schmid, W. E.; Kompa, K.-L. *J. Phys. Chem. A* **1998**, *102*, 9334.
(38) Joo, T.; Albrecht, A. C. *Chem. Phys.* **1993**, *173*, 17.
(39) Freed, K. F. In *Radiationless Processes in Molecules and Condensed Phases;* Fong, F. K., Ed.; Topics in Applied Physics; Springer-Verlag: Berlin, 1976; Vol. 15, p 23.
(40) Steinfeld, J. I.; Francisco, J. S.; Hase, W. L. *Chemical Kinetics and Dynamics*; Prentice Hall: Englewood Cliffs, NJ, 1991; p 308.
(41) Rosker, M. J.; Dantus, M.; Zewail, A. H. *Science* **1988**, *241*, 1200.
(42) Cheng, P. Y.; Zhong, D.; Zewail, A. H. *Chem. Phys. Lett.* **1995**, *237*, 399.
(43) Fuss, W.; Schmid, W. E.; Trushin, S. A. *J. Chem. Phys.* **2000**, *112*, 8347.
(44) Rodríguez Prieto, M. F.; Nickel, B.; Grellmann, K. H.; Mordziński, A. *Chem. Phys. Lett.* **1988**, *146*, 387.
(45) Nickel, B.; Walla, P. J. *Chem. Phys.* **1998**, *237*, 371.
(46) Wiechmann, M.; Port, H. *J. Lumin.* **1991**, *48/49*, 217.
(47) Heller, E. J.; Sundberg, R. L.; Tannor, D. *J. Phys. Chem.* **1982**, *86*, 1822.
(48) Pfeiffer, M.; Lenz, K.; Lau, A.; Elsaesser, T. *J. Raman Spectrosc.* **1995**, *26*, 607.
(49) Pfeiffer, M.; Lenz, K.; Lau, A.; Elsaesser, T.; Steinke, T. *J. Raman Spectrosc.* **1997**, *28*, 61.
(50) Zinth, W.; Leonhardt, R.; Holzapfel, W.; Kaiser, W. *IEEE J. Quantum Electron.* **1988**, *24*, 455.
(51) Pollard, W. T.; Lee, S.-Y.; Mathies, R. A. *J. Chem. Phys.* **1990**, *92*, 4012.
(52) Douhal, A.; Lahmani, F.; Zehnacker-Rentien, A.; Amat-Guerri, F. *J. Phys. Chem.* **1994**, *98*, 12198.